Available online at www.sciencedirect.com

SciVerse ScienceDirect

Scripta Materialia 67 (2012) 455–458

Scripta MATERIALIA

www.elsevier.com/locate/scriptamat

μ-CT-based finite element analysis on imperfections in open-celled metal foam: Mechanical properties

T. Fiedler,* I.V. Belova and G.E. Murch

The University of Newcastle, Building ES, 4th Floor, Callaghan, NSW 2308, Australia

Received 7 May 2012; revised 1 June 2012; accepted 3 June 2012
Available online 16 June 2012

This study digitally identifies and repairs defects produced in the manufacturing of an open-cell metal foam for the first time. Finite element calculations are based on microcomputed tomography data of actual samples. The effective Young's modulus and 0.2% offset yield strength are calculated and equivalent plastic strain is used to identify weakness within the material. In areas of high plastic deformation, the structure is digitally repaired locally and the calculations are repeated in order to quantify the change in material properties.

Keywords: Cellular material; Imperfection; Finite element analysis; Three-dimensional tomography

Cellular metals are multifunctional materials that combine high specific stiffness and strength [1,2] with structural damping [3], versatile thermal properties [4,5], large internal surface area and excellent energy absorption [6,7]. However, their properties are quite variable as a result of defects produced during manufacturing. This is proving to be a major impediment in their large-scale application [8]. The present work investigates the impact of small geometric imperfections, such as thin or damaged struts which are produced in manufacturing, on the macroscopic material properties for the first time. The aim of the study is the identification of critical defects to facilitate the design of stronger, more reliable cellular metals.

The mechanical properties of cellular metals have been the subject of intensive research. Generally speaking, two types of cellular metals are distinguished: those with closed and those with interconnected porosity. The present paper addresses open-celled M-Pore® aluminium, which falls into the latter category (see Fig. 1). Its cellular structure is formed by interconnected struts with approximately circular cross-sections. A classification system for mathematical morphology based on Minkowski functionals was proposed in Ref. [9]. Based on this system, the considered material has the following averaged functionals: a relative density $V = 0.10$, a normalized surface area $S = 1.23$, a normalized mean breadth $B = 1.44$ and a normalized Euler characteristic $\chi = 35.5$.

Previous analysis of such material has been extensive, and includes experimental [10,11], analytical [12] and numerical [13,14] approaches. Numerical analysis uses both simplified model structures [15] and, more recently, highly accurate calculation models that are derived from microcomputed tomography (μ-CT) data [13,16]. The latter allows the consideration of the complex, random mesostructure of the material, and is also used in the present analysis. Imperfections in open-celled metals were previously considered in Ref. [17], where wire-woven cellular metal was investigated. Wire-woven cellular metals are manufactured in a three-dimensional weaving process using helical metallic wires. Unlike the presently investigated stochastic M-Pore® foam, they exhibit a mostly periodic geometry. Combined finite element and network analysis was applied to understand the change in mechanical behaviour due to the imperfections. A perturbation was introduced by shifting the joints of regular starting geometries. The effective material strength was found to gradually decrease with increasing levels of imperfection. In Ref. [18], regular model structures were perturbed by randomly shifting or removing struts; however, the shape of the struts remained unchanged. In accordance with previous work, a decrease in elastic stiffness and material strength was found for increasing disorder. Finite element analysis on open-cell metal foam was conducted in Ref. [19], using non-periodic tetrakaidecahedral model structures. Perturbations were introduced by removing struts, curving struts or filling faces within the material. Curved struts were found to have a minor impact on mechanical

* Corresponding author. E-mail: Thomas.Fiedler@newcastle.edu.au

1359-6462/$ - see front matter
http://dx.doi.org/10.1016/j.scriptamat.2012.06.002

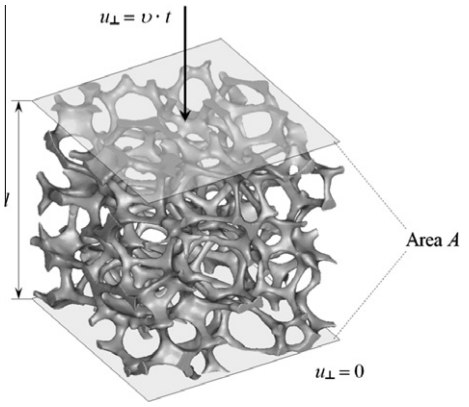

Figure 1. M-Pore® calculation model No. 1 with boundary conditions.

properties, whereas distinct decreases in stiffness and strength were observed for missing struts. Strain-induced damage was considered in Refs. [20–22]. Open-cell Duocel® aluminium foam (20 pores per inch) was investigated and the change in electrical resistance during loading was related to load-induced damage. Results indicate that damage accumulation starts well before the peak strain is reached. Damage accumulation was found to depend both on the relative density and the heat treatment of the samples. It should be emphasized here that the present work focuses on defect damage produced by the manufacturing process that affects material behaviour prior to the damage caused by material deformation.

The present paper supplements previous research and takes it an important step further. For the first time, the simplified model structures that have been used in previous research are replaced by CT data. The major advantage in using CT data is the substitution of artificial perturbations by actual geometric data that accurately represents the defects introduced by manufacturing. To this end, finite element analysis is conducted based on μ-CT data. Simulation results are used to identify local concentrations of plastic deformation caused by critical imperfections. These imperfections are digitally removed and simulations are repeated in order to scrutinize their impact on the macroscopic material behaviour. This is a paradigm shift in approach to identifying the causes of the variability of properties of open-cell metal foams.

Finite element analysis was used to investigate the effective mechanical properties and mesostructure deformation of open-cell M-Pore® metal foam. Finite element calculation models were based on the geometry of real samples. To this end, μ-CT scans of real samples were performed. The three-dimensional (3-D) CT image acquisition was performed using a Xradia MicroXCT-400 CT system. An accelerating voltage of 120 kV and a current of 70 μA were used for the radiography of the M-Pore® specimens. The radiographies were conducted using the Hamamatsu L8121-03 X-ray source. During the irradiation of the samples, 1801 2-D projections were acquired using an exposure time of 2 s and a resolution of 50.13 μm voxel^{-1}. The 3-D volume processing was applied to the projections of the 2-D radiography images. For the 3-D reconstruction, the software XMReconstructor from Xradia was used. For better contrast conditions between metal and pores, image processing based on a median filtering was performed. Three different samples with dimensions $20 \times 50 \times 100$ mm were captured. The finite element meshes comprised non-intersecting cubes extracted from these scans with a side length of 20 mm. A total of eight different samples were considered. Each geometry contains five cells per edge, which is commonly regarded as being sufficiently large to constitute a representative volume [23]. The focus is the comparative study of real imperfections, thus a relatively small geometry size is beneficial since it strengthens the impact of imperfection on macroscopic properties. The study of imperfection density and mechanical properties is considered elsewhere [18,19], and is not the aim of the present analysis. In order to eliminate size effects, only one imperfection per identically sized geometry is considered at any time unless otherwise indicated. In the following, the original geometries are labelled as μCT, and geometries in which one major imperfection was digitally repaired are designated modified. In addition, an optimized geometry is considered where all major imperfections have been repaired in order to estimate the maximum potential of M-Pore® foam.

The geometry data was converted into mixed finite element meshes containing linear hexahedral, linear tetrahedral and linear pentahedral elements, which have been shown to yield superior accuracy [24]. The commercial software package MSC.Marc was used for the finite element analysis. The corresponding MSC.Marc element numbers are 43, 135 and 137. A multifrontal sparse solver was used for the solution of the equation system. Due to the large size of the calculation models (i.e. containing in excess of 1.35×10^6 elements), high-performance computers with 64 GB RAM were used for the numerical analysis. The average computation time per model was 155 h.

Uniaxial compressive loading of the specimens was simulated. To this end, normal displacement was constrained within one of the surfaces (see Fig. 1). Within the opposing surface of the cubic sample, quasi-static displacement was prescribed incrementally within 500 time steps. To this end, a time t dependent normal displacement $u_\perp = v \times t$ was defined, where the parameter v is small enough to avoid the occurrence of dynamic effects. M-Pore® foam exhibits weak anisotropy in its properties [25] so, in order to eliminate any directional influence, all the structures were loaded in the same direction. The base material of the struts is aluminium, i.e. Young's modulus $E_{Al} = 70$ GPa, Poisson's ratio $\nu = 0.33$ and the yield stress $\sigma_y = 200$ MPa. For the base material, ideal plasticity was presumed.

Finite element results were evaluated using a subroutine that calculates technical stresses and strains parallel and perpendicular to the loading direction. For the calculation of technical stress and strain, the reference area A and length l, respectively, are shown in Figure 1. Young's modulus is the constant gradient of technical stress as a function of strain in the loading direction within the elastic range $E = \sigma_{\|}/\varepsilon_{\|}$. The 0.2% offset yield strength $\sigma_{0.2}$ is determined as the stress at which 0.2% plastic deformation remains after the unloading of the structure.

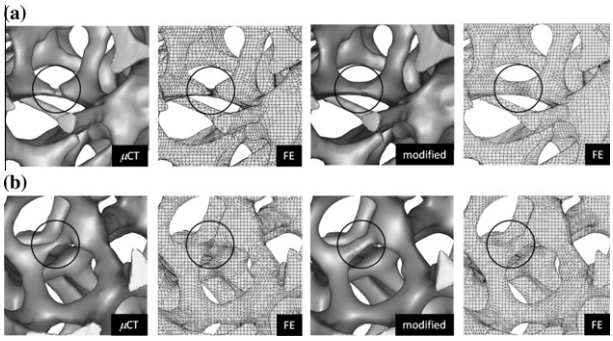

Figure 2. μ-CT geometry (first column), equivalent plastic strain (second column), modified geometry (third column) and equivalent plastic strain (fourth column) for (a) sample No. 4 and (b) sample No. 5.

The evaluation of calculation results also includes the analysis of the distribution of plastic deformation. To this end, the equivalent plastic strain is visualized as a contour map projected onto the surface of the 3-D calculation models (see Fig. 2). High levels of equivalent plastic deformation are indicated by dark grey, whereas light grey corresponds to purely elastic deformation. Structural imperfections were identified as local concentrations of plastic deformation. In Figure 2, two different types of imperfections are shown as μ-CT geometry (first column), surface maps of plastic deformation (second and fourth columns) and reinforced modified geometry (third column). In the top row (a), a notch causes stress concentration within a strut. In the modified structure, this notch is digitally filled to reinforce the strut. In the second row (b), a thin strut is unable to bear the loads distributed within the structure. In the modified structure, the diameter of the strut is increased in order to decrease the local stress and plastic deformation.

Preliminary mesh refinement analysis ensures numerical convergence of the calculation models. To this end, six calculation models of sample No. 2 were generated using increasing numbers of elements. For each of these models, uniaxial compressive loading was simulated and the stress–strain responses were recorded (see Fig. 3a). Young's moduli and 0.2% offset yield strengths were also determined (see Fig. 3b). Analysis of the results indicates that good numerical convergence is achieved at the second highest mesh density, containing approximately 1.35×10^6 elements. Subsequent results are presented for meshes containing similar mesh densities with minor changes of element numbers due to small variations in porosity.

Calculations were first conducted for the geometries obtained by μ-CT scanning. Figure 4a shows the technical stress–strain plots of the μ-CT finite element models. Samples are numbered in ascending order with respect to their porosity, i.e. No. 1 has the lowest and No. 8 the highest porosity. It can be observed that stress levels decrease with increasing porosity. Based on the stress–strain data, the effective material parameters Young's modulus E and 0.2% offset yield strength $\sigma_{0.2}$ are extracted. The results are plotted vs. porosity in Figure 4b. In addition, two experimental data points of the material strength are added and good agreement with simulation results is found. The trend observed in Figure 4a is confirmed: both Young's modulus and the 0.2% offset yield strength decrease with increasing porosity. However, closer examination of the data reveals a certain degree of scattering for both material parameters. In the following, analysis of the mesostructure is used to relate the variation in properties to small geometric imperfections of the struts.

In the next step, the distribution of equivalent plastic strain was analysed. With the exception of sample Nos. 3 and 8, localized concentrations of plastic strain could be observed. Following the procedure demonstrated in Figure 2, struts were digitally reinforced by filling in the notches (sample Nos. 2 and 4) or increasing the strut diameter. The geometry modifications change the overall porosity. However, the decrease in porosity in all cases is smaller than 0.001, which is negligible. For each

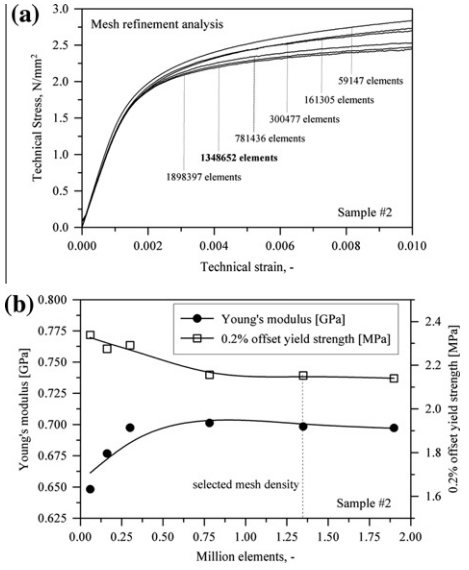

Figure 3. Mesh refinement analysis: (a) stress–strain; (b) effective material properties.

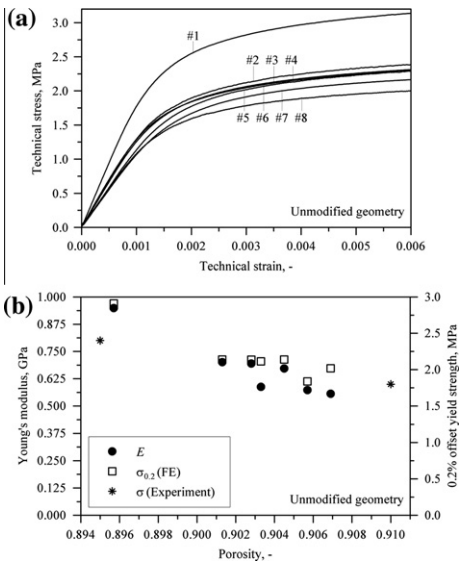

Figure 4. μCT geometries: (a) stress–strain data; (b) material properties (experimental values taken from Ref. [26]).

Table 1. Material properties of μ-CT and modified geometries.

No	Major defect	μ-CT (MPa)		Modified (MPa)		Change	
		E	$\sigma_{0.2}$	E	$\sigma_{0.2}$	E(%)	$\sigma_{0.2}$
1	Thin strut	950	2.91	955	2.91	0.3	–
2	Notch	690	2.14	700	2.17	1.6	1.3
3	–	730	2.10	–	–	–	–
4	Notch	725	2.11	750	2.23	3.2	5.7
5	Thin strut	590	2.11	590	2.13	–	0.5
6	Thin strut	670	2.14	675	2.19	0.7	2.2
7	Thin strut	575	1.84	585	1.90	1.7	3.3
8	–	560	2.02	–	–	–	–

model, only the defect with the highest plastic deformation was considered. Calculations were repeated with the modified geometries under otherwise identical conditions to isolate the change in material behaviour due to the single defect. The results are summarized in Table 1.

In all cases, an improvement in Young's modulus and/or 0.2% offset yield strength can be observed after geometry modification. This increase is more pronounced for the offset yield strength. It can be concluded that even small geometric imperfections can have a distinct impact on macroscopic properties and are probably responsible for the material property variations, as shown, for example, in Figure 4. The greatest change is found for sample No. 4, with a 3.2% increase in Young's modulus E and a 5.7% increase in $\sigma_{0.2}$. It should be mentioned here that the sample size considered (8) is too low to provide statistically safe information. However, there is some indication that notch defects are more critical than thin struts in causing a higher decrease in stiffness and strength.

Up to this point, only a single geometric defect per model was considered in order to avoid distortion of the imperfection significance due to size effects. However, in order to estimate the full potential of M-pore® aluminium foam, one geometry must be further optimized. To this end, the modified geometry of sample No. 4 is considered. In contrast to previous geometric modifications, not one but all major imperfections were digitally repaired. Geometric changes are limited to these areas and the resulting optimized geometry has a porosity $p = 0.902$, similar to the original μ-CT porosity of $p = 0.903$. Distinct increases in stiffness $E = 790$ MPa (+8.4%) and, in particular, offset yield strength $\sigma_{0.2} = 2.50$ MPa (+18.6%) are found for the optimized geometry. The results of the optimized geometry can be considered as representing an upper estimate for the material behaviour of random open-celled metal foam without critical structural defects.

Micro-CT scans of M-Pore® aluminium foam were obtained and converted into geometrically accurate finite element models. Numerical analysis of these calculation models was conducted and the effective Young's modulus and 0.2% offset yield strength were determined. In addition, concentration of equivalent plastic strain was used to identify structural imperfections. Computed tomography data was modified by digitally removing a single imperfection within each model. The finite element analysis was repeated in order to quantify the change in macroscopic properties. It was found that even small changes in the mesostructure can have a pronounced effect at the macroscale. Due to limited CT data in combination with very long calculation times, only a relatively small number of eight samples and imperfections were considered, thus reducing the statistical significance of the results. However, the results suggest that notches within the struts cause the highest decrease in effective Young's modulus and 0.2% offset yield strength. Finally, one selected model was further optimized by removing all imperfections. Strong increases in stiffness (+8.4%) and strength (+18.6%) were found, providing an estimate for the full potential of defect-free open-celled cellular metal.

[1] J. Banhart, Prog. Mater. Sci. 46 (2001).
[2] M.F. Ashby, A.G. Evans, N.A. Fleck, L.J. Gibson, J.W. Hutchinson, H.N.G. Wadley, Properties of Metal Foams, Butterworth-Heinemann, Burlington, MA, 2000 (Ch. 4).
[3] I.S. Golovin, H.R. Sinning, I.K. Arhipov, S.A. Golovin, M. Bram, Mater. Sci. Eng. A 370 (2004).
[4] T. Fiedler, E. Solórzano, F. Garcia-Moreno, A. Öchsner, I.V. Belova, G.E. Murch, Mater. Sci. Eng. Technol. 40 (2009) 139.
[5] T. Fiedler, I.V. Belova, G.E. Murch, Comp. Mater. Sci. 50 (2010) 503.
[6] S. Tanaka, K. Hokamoto, S. Irie, T. Okano, Z. Ren, M. Vesenjak, S. Itoh, Measurement 44 (2011).
[7] M. Vesenjak, L. Krstulović-Opara, Z. Ren, A. Öchsner, Ž. Domazet, Exp. Mech. 49 (2009) 501.
[8] U. Ramamurty, A. Paul, Acta Mater. 52 (2004).
[9] K. Michielsen, H.D. Raedt, J.T.M. de Hosson, Adv. Imaging Electron Phys. 125 (2002).
[10] W.-Y. Jang, S. Kyriakides, Int. J. Solids Struct. 46 (2009).
[11] X. Badiche, S. Forest, T. Guibert, Y. Bienvenu, J.D. Bartout, P. Ienny, M. Croset, H. Bernet, Mater. Sci. Eng. A 289 (2000).
[12] H.X. Zhu, J.F. Knott, N.J. Mills, J. Mech. Phys. Solids 45 (1997).
[13] C. Veyhl, I.V. Belova, G.E. Murch, T. Fiedler, Mater. Sci. Eng. A 528 (2011) 4550.
[14] Y. An, C.E. Wen, P.D. Hodgson, C. Yang, Comp. Mater. Sci. 55 (2012).
[15] T. Fiedler, A. Öchsner, J. Grácio, G. Kuhn, Mech. Compos. Mater. 41 (2005) 405.
[16] I. Jeon, T. Asahina, K.-J. Kang, S. Im, T.J. Lu, Mech. Mater. 42 (2010).
[17] S. Hyun, J.-E. Choi, K.-J. Kang, Comp. Mater. Sci. 46 (2009).
[18] M.H. Luxner, J. Stampfl, H.E. Pettermann, Comp. Mater. Sci. 47 (2009).
[19] Z.-X. Lu, Q. Liu, J.-X. Huang, Mater. Sci. Eng. A 530 (2011).
[20] E. Amsterdam, J.H.B. de Vries, J.T.M. de Hosson, P.R. Onck, Acta Mater. 56 (2007).
[21] E. Amsterdam, J.T.M. de Hosson, P.R. Onck, Scripta Mater. 59 (2008).
[22] E. Amsterdam, H. van Hoorn, J.T.M. de Hosson, P.R. Onck, Adv. Eng. Mater. 10 (2008).
[23] A.P. Roberts, E.J. Garboczi, Proc. R. Soc. 458 (2000) 1033.
[24] C. Veyhl, I.V. Belova, G.E. Murch, A. Öchsner, T. Fiedler, Finite Elem. Anal. Des. 46 (2010) 371.
[25] M. Vesenjak, C. Veyhl, T. Fiedler, Mater. Sci. Eng. A 541 (2012) 105.
[26] D. Girlich, C. Kühn, K. Hackeschmidt, Konstruktion 9 (2004) 69.